crystals

MDPI

Article

Pharmaceutical Cocrystal Development of TAK-020 with Enhanced Oral Absorption

Kouya Kimoto [1,*], Mitsuo Yamamoto [1], Masatoshi Karashima [1], Miyuki Hohokabe [2], Junpei Takeda [1], Katsuhiko Yamamoto [1] and Yukihiro Ikeda [1]

[1] Analytical Development, Pharmaceutical Sciences, Takeda Pharmaceutical Company Limited, 26-1, Muraoka-Higashi 2-Chome, Fujisawa, Kanagawa 251-8555, Japan; mitsuo.yamamoto@takeda.com (M.Y.); masatoshi.karashima@takeda.com (M.K.); junpei.takeda@takeda.com (J.T.); katsuhiko.yamamoto@takeda.com (K.Y.); yukihiro.ikeda@takeda.com (Y.I.)

[2] Drug Product Development, Pharmaceutical Sciences, Takeda Pharmaceutical Company Limited, 26-1, Muraoka-Higashi 2-Chome, Fujisawa, Kanagawa 251-8555, Japan; miyuki.hohokabe@takeda.com

* Correspondence: kouya.kimoto@takeda.com; Tel.: +81-466-32-2858

Received: 17 February 2020; Accepted: 16 March 2020; Published: 18 March 2020



Abstract: The objective of this study was to improve the solubility of poorly water-soluble drugs by pharmaceutical cocrystal engineering techniques and select the best pharmaceutical forms with high solubility and solubilized formulations for progress from the early discovery stage toward the clinical stage. Several pharmaceutical cocrystals of TAK-020, a Bruton tyrosine kinase inhibitor, were newly discovered in the screening based on the solid grinding method and the slurry method, considering thermodynamic factors that dominate cocrystal formation. TAK-020/gentisic acid cocrystal (TAK-020/GA CC) was selected based on a physicochemical property of enhanced dissolution rate. TAK-020/GA CC was proven to be a reliable cocrystal formation with a definitive stoichiometric ratio by a variety of analytical techniques—pKa calculation, solid-state nuclear magnetic resonance, and single X-ray structure analysis from the view of regulation. Furthermore, its absorption was remarkable and beyond those achieved in currently existing solubilized formulation techniques, such as nanocrystal, amorphous solid dispersion, and lipid-based formulation, in dog pharmacokinetic studies. TAK-020/GA CC was the best drug form, which might lead to good pharmacological effects with regard to enhanced absorption and development by physicochemical characterization. Through the trials of solid-state optimization from early drug discovery to pharmaceutical drug development, the cocrystals can be an effective option for achieving solubilization applicable in the pharmaceutical industry.

Keywords: cocrystal; poorly soluble drug; crystal engineering; solubilized formulation; absorption improvement

1. Introduction

The oral route is the most common used for drug administration and is the first priority in pharmaceutical development. Nearly 40% of marketed drugs and 70% of drug candidates in current pharmaceutical development exhibit poor aqueous solubility. Aqueous solubility is one of the most important physicochemical properties for the success of oral dosage formulations, since poor aqueous solubility leads to low oral bioavailability and pharmacokinetic (PK) variability, resulting in insufficient therapeutic efficacy and limited exposure in toxicological studies [1–3]. Hence, poor aqueous solubility of drugs often needs to be solved through pharmaceutical development. Numerous technologies, including crystal engineering, formulation, and both of these in combination were investigated for enhancing solubility and the dissolution rate. The rational selection of these technologies for

pharmaceutical drug development is therefore required while strongly considering the associated advantages and disadvantages, including, for physicochemical properties, stability, bioavailability, safety, cost, and manufacturability [4,5]. Salt formation, which has been applied to many marketed drugs, is a primary approach to modifying a drug's physicochemical properties by changing the molecular interactions of its active pharmaceutical ingredient (API); however, applicable APIs are limited due to their requirement for a suitable ionizable site [6]. A generally successful approach for selecting applicable techniques has not yet been established because which technique is appropriate depends on the physicochemical and chemical properties of the APIs. Known solubilized formulations, such as amorphous solid dispersion (ASD), lipid-based formulation (LBF) and cyclodextrin (CD) inclusion complex for improving the solubility; and nanocrystal (Nanocry) for improving the dissolution rate, also have limitations due to numerous concerns, such as difficulty of formulation preparation and manufacturability, inflexibility of dose, and instability of shelf life; success is not always achieved. Namely, to successfully enhance oral bioavailability of APIs, repeated trial and error is required, with these approaches still remaining a challenge [4,7]. Accordingly, other novel technologies for enhancing solubility, such as cocrystal, coamorphous, and nano-cocrystal systems have been studied to overcome the problem of low aqueous solubility in pharmaceutical drug development [5,8–10].

A cocrystal is defined as a multi-component crystal structured through non-ionic interactions with a specific stoichiometric ratio; it is composed of an API and a pharmaceutically acceptable cocrystal former (CCF) linked mainly by hydrogen bonding. Unlike salts, almost all APIs have potential for co-crystallization because they have substantial hydrogen bonding sites [11,12]. Over the last decade, many reports about cocrystals have been published in the field of pharmaceutical sciences because of their abilities to improve physicochemical properties, such as crystallinity, melting point, dissolution, hygroscopicity, stability, and solubility [12–14]. The achievements in these studies have led to a deep understanding of rational cocrystal formation based on solution, slurry, grinding, and melting [15–17]; data are also available on motifs for interactions with CCFs to estimate the forming cocrystal for the trial trigger of a cocrystal application [18]. These contributions have enabled the establishment of high-throughput screening, leading to a small number of APIs being selected at the early drug discovery stage in pharmaceutical companies [19–21]. Although the pharmaceutical development strategy of a drug product has to be selected among various solubilized technologies, little to no comparison between the cocrystals and solubilized formulations has been made in pharmaceutical drug development.

Additionally, as strategic tools for pharmaceutical companies, cocrystals are profoundly important from clinical, legal, and regulatory perspectives, since they are patentable when they satisfy the criteria of novelty, industrial applicability, and non-obviousness. At the regulatory level, the United States Food and Drug Administration (FDA) and the European Medicines Agency published regulatory guidelines on the requirements to definitively classify cocrystals in pharmaceutical solid forms. In particular, FDA guidance states that the pKa difference of 1 or less between API and CCF is important to proving a new formation as a cocrystal, unlike salt [22,23]. In pharmaceutical cocrystal development, there is a requirement for proof of cocrystal formation by non-ionic interactions, in accordance with the guidelines. In addition, physicochemical charact-erization by reliable analysis is also required in order to ensure cocrystal performance and quality control [24,25]. Currently, there are few cocrystal products on the market or in clinical trials. In the translational development of cocrystal to drug, there may be more challenges than usual regarding polymorphism, manufacturing, and formulation, which inhibit cocrystal drug development [26]. Along with the publication of regulatory guidelines, the understanding of physicochemical properties, cocrystal structure, and pharmaceutical performance from the early drug discovery stage is indispensable for the successful development of cocrystal drugs; however, both the cocrystal engineering of a new API, and the actual R&D initiatives, including the comparison between cocrystal and other formulations techniques, have not been reported yet.

TAK-020, a Bruton tyrosine kinase inhibitor, was discovered by Takeda California as a drug for the treatment of rheumatoid arthritis via oral administration [27]. TAK-020 has low aqueous solubility,

and cationic salt formation to enhance its solubility was found not to produce an adequate solid form due to its chemical instability. Captisol® (sulfobutylether-β-cyclodextrin; SBE-β-CD) has been used for preclinical studies to enhance solubility. Captisol® is a chemically modified CD that is widely used as a pharmaceutical excipient. Although CD has been well tolerated, the side-effects following oral treatment with various CDs or their derivatives have been reported to be soft feces or diarrhea, and cecal enlargement depending on the amount used [28]. Therefore, the cocrystal approach would be useful for developing a better medicine for patients without any excipients.

Taken together, the purpose of this study was to enhance oral absorption of TAK-020 by means of cocrystal approach, taking translational development into account. A suitable TAK-020 cocrystal was developed through a series of cocrystal screenings and physicochemical characterization, and an in vivo PK study after the oral administration of the consequently selected TAK-020 cocrystal was conducted. Briefly, TAK-020 cocrystal screening was performed by using three high-throughput screening techniques (conventional reaction crystallization and original theoretically designed methods of grinding and slurry). In the course of physicochemical characterization, the most suitable cocrystal was determined from the viewpoint of dissolution performance and CCF clinical applicability. The selected cocrystal was analyzed to meet the regulatory guidelines by multi-sided analysis techniques using calculation of pKa difference, solid-state nuclear magnetic resonance (NMR), and single X-ray structure analysis. Finally, the in vivo PK studies of selected cocrystal and other solubilized formulations were performed to determine the translational solid form for drug development.

2. Materials and Methods

2.1. Materials

TAK-020(5-(1-{[(3*S*)-1-(prop-2-enoyl)pyrrolidin-3-yl]oxy}isoquinolin-3-yl)-2,4-dihydro-3*H*-1,2,4-triazol-3-one) was synthesized by Takeda California, Inc. (San Diego, CA, USA). Ethylmaltol, lactamide, and hippuric acid were purchased from Tokyo Kasei Kogyo (Tokyo, Japan). Glycoamide and microcrystalline cellulose were purchased from Sigma-Aldrich (St. Louis, MO, USA). Hydroxypropyl methylcellulose phthalate HP-55 (HPMCP HP-55) and hydroxypropyl cellulose (HPC) were purchased from Shin-Etsu Chemical (Tokyo, Japan). Sodium starch glycolate (Primojel®) was purchased from DFE Pharma (Goch, Germany). Silicic acid (Aerosil® 200) was purchased from Evonik (Essen, Germany). Glyceryl monocaprylate (Capmul® MCM C8) was purchased from ABITEC (Columbus, OH, USA). Croscarmellose sodium (AcDiSol®) was purchased from FMC Health and Nutrition (Philadelphia, PA, USA). D-Mannitol was purchased from Roquette Pharma (Lestrem, France). Docusate sodium was purchased from Cytec Industries, Inc. (Blemont, WV, USA). The other CCFs, deuterium oxide (D_2O) and 3-(trimethylsilyl) propionic-2,2,3,3-d4 acid sodium (TSP-d4), excipients, and all solvents were purchased from Wako Pure Chemical Industries (Osaka, Japan). TAK-020/gentisic acid cocrystal (TAK-020/GA CC) for PK study was provided by Takeda Pharmaceutical Company Limited (Osaka, Japan). All other chemicals were of the highest grade commercially available, and all solutions were prepared in deionized distilled water.

2.2. Cocrystal Screening

Cocrystal screenings of TAK-020 were performed using 29 types of CCFs (Table 1) by three different methods based on reaction crystallization, solid grinding, and slurry aging. Twenty-nine types of CCFs were selected based on structural diversity and computationally obtained ΔpKa values with 1 or less between TAK-020 (pKa 2.33 using ACD Labs version 12.01) and each CCF. These CCFs have already listed in monographs as counter for acids and bases of salt [29]. Solvents were selected considering the diversity of different dissolved amounts of API and CCF, and solvent properties. Trifluoroethanol (TFE) was used to enhance dissolved amount of TAK-020 for reaction crystallization. Solvent volume was set to completely dissolve TAK-020 for reaction crystallization and to make suspension for slurry

aging, respectively. Cocrystal screenings of three different methods and the diversity of CCFs and solvents provided comprehensive conditions maintaining the high-throughput.

2.2.1. Conventional Reaction Crystallization (CRC)

TAK-020 was dissolved in a mixed solution of dimethyl sulfoxide (DMSO)/1,4-dioxane (1:2, v/v) to make a 3.3 mg/mL solution. This API solution was then added to a 96-well crystallization plate (Unchained Labs, USA) to make ca. 1 mg/well. CCF solution in 1,4-dioxane equivalent to a 1.05 molar ratio to API was also added to the 96-well crystallization plate. API and CCF solutions in the 96-well crystallization plate were frozen at − 40 °C and solvents were completely removed by lyophilization for 24 h. Then, 250 µL of acetonitrile (ACN) and mixed solutions of TFE/acetone, TFE/chloroform, and TFE/tetrahydrofuran (1:1, v/v) were dispersed into each well at 250 µL. Mini stirrer bars were added to each well, and the 96-well crystallization plate was slowly cooled at 3 °C per h from 25 °C to 5 °C for crystallization while stirring at 500 rpm. The plate assembly was opened after completing solvent evaporation using a nitrogen gas flow in all wells and the resultant powder was obtained.

2.2.2. Cocktail Cocrystal Grinding (CCG)

About 10 mg of TAK-020 with cocktail CCFs were physically mixed with each equivalent molar CCF having a similar functional group [20,29]. They and two 6 mm stainless-steel balls were placed in a 2.0 mL polypropylene vial. Then, 7.5 µL of ACN, ethanol, or n-heptane was added to the vial. The vial was shaken by Shake Master Neo Mixer Mill (Biomedical Science, Inc.) at 1500 rpm for 5 min. The resultant powder was collected from the vial. Re-grinding was carried out with individual CCF to identify the CCF of cocrystal formation.

2.2.3. Saturated CCF Solution Slurry (SCS)

TAK-020 was dissolved in TFE and the solution was dispersed into a 96-well crystallization plate with 2 mg of API/400 µL solvent per well. Then, the TFE was completely removed by nitrogen gas flow. CCFs were suspended in ACN, ethyl acetate, ethanol, or ethanol/water (1:1, v/v) and were left to stand to make the CCF saturation solution a supernatant for 1 day after stirring with a stirrer bar at 250 rpm for 1 h. A total of 50 µL of each saturated CCF solution was dispersed into the well and stirred with mini stirrer bars for 3 days. If some wells resulted in a solution state after 2 days, 50 µL of anti-solvent of n-heptane, toluene, water, or 2-propanol, which is miscible with the corresponding solvent, was added to the well. The plate assembly was opened after completing solvent evaporation using a nitrogen gas flow in all wells and the resultant powder was obtained.

2.3. Cocrystal Powder Preparation

Citric acid (CA), malonic acid (MoA), maleic acid (MeA), L-malic acid (MaA), (+/−)-mandelic acid (MdA), gentisic acid (GA), and salicylic acid (SA) were suspended in ACN and left to stand to make the CCF saturation solution a supernatant for 1 day after stirring with a stirrer bar at 250 rpm for 1 h. TAK-020 was suspended in each saturated CCF ACN solution and the slurry was stirred with a stirrer bar for 5 days at ambient temperature (ca. 25 °C). TAK-020 suspensions in CCF ACN solution were filtered off by a vacuum and the resulting solid was collected and completely dried.

2.4. Powder X-Ray Diffractometry (PXRD)

PXRD patterns were collected using an Ultima IV (Rigaku Corporation, Tokyo, Japan) with Cu-Kα radiation generated at 40 kV and 50 mA. The powder placed on a silicon sample plate was analyzed with an X-ray powder diffractometer. Data were collected from 2° to 35°(θ) at increments of 0.02° and scanning speed of 6°/min.

2.5. Thermal Analysis

Thermogravimetry (TG) was performed using a TGA/DSC1 system (Mettler-Toledo Interna-tional Inc., Greifensee, Switzerland). TG curves were obtained in an aluminum pan at a heating rate of 5 °C/min under a nitrogen gas flow. Differential scanning calorimetry (DSC) was performed using a DSC1 system (Mettler-Toledo International Inc., Greifensee, Switzerland). DSC curves were obtained in a crimped aluminum pan at a heating rate of 5 °C/min under nitrogen gas flow.

2.6. Dissolution Test

Dissolved amount was measured by the shake flask method [1]. Samples were weighed into Thomson filter vials (Chrom Tech, Inc., Minnesota, USA) containing a 0.45 μm polyvinylidene difluoride filter membrane. A total of 400 μL of Japanese Pharmacopoeia, 17th edition, disintegration 1st and 2nd test fluid (JP1, pH 1.2), JP2 (pH 6.8), fasted state simulated intestinal fluid version 2 (FaSSIF), and fed state simulated intestinal fluid (FeSSIF) were added to the vials [30]. The vials were incubated at 37 °C with shaking at 500 rpm for 2 h and were filtrated by compressing them. Dissolved amount was determined by high-performance liquid chromatography (HPLC).

2.7. Intrinsic Dissolution Rate (IDR)

IDRs were measured using a rotating disk method [31]. Samples were compressed at a force of 20 kN/cm^2 using a single-punch tablet press (Riken Seiki, Tokyo, Japan) to obtain 7-mm-diameter disks. The disks were attached to the axis of the dissolution test and rotated in 250 mL of JP2 containing 200 mmol/L sodium cholate at 200 rpm; the temperature of the dissolution medium was kept at 37 °C. At each time interval, 0.50 mL of the solution was withdrawn and the drug concentration was determined by HPLC.

2.8. In Vitro Dissolution-Permeation Study

In vitro dissolution-permeation studies were performed using μFLUX (pION Inc., Boston, MA, USA). The apparatus consisted of donor and receiver chambers separated by an artificial membrane of polyvinylidenfluoride, coated with gastrointestinal tract lipid solution. A total of 16 mL of TAK-020/GA CC suspension in FaSSIF at 0.4 mg/mL as TAK-020 free and 16 mL of acceptor sink buffer (pH7.4; pION Inc., Boston, MA, USA) at 37 °C were added to the donor and receiver chambers, respectively. At each time interval, 0.15 mL of the sample aliquots was withdrawn while stirring at 150 rpm and the supernatant was obtained after centrifugation for 15 min at 13,000 rpm and diluted for HPLC analysis. The TAK-020 and GA concentrations in the donor and receiver chambers were quantified by HPLC.

2.9. HPLC

Quantitative analysis was conducted using a ultra HPLC system of Prominence UFLC (Shimadzu Corp., Kyoto, Japan) with a photodiode array detector operated at 250 nm. A YMC-UltraHT Pro C18 packaged column (2 μm, 2.0 × 30 mm; YMC Co., Ltd., Kyoto, Japan) was used at 40 °C with gradient programs. The mobile phase was distilled water/50 mM ammonium acetate buffer/ACN (8:1:1, v/v/v) (A) and 50 mM ammonium acetate buffer/ACN (1:9, v/v) (B) at a flow rate of 0.7 mL/min. The starting mobile phase consisted of 95% A and 5% B for 0.1 min, changed gradually to 5% A and 95% B from 0.1 to 1.6 min, and then returned to the initial condition after 1.3 min and was re-equilibrated for an additional 0.6 min.

2.10. NMR Spectroscopy

^{13}C NMR and ^{15}N NMR spectra were collected using a JNM-ECX500II (JEOL RESONANCE, Japan) with a magnetic field strength of 11.7 T. A 3.2 mm HX MAS probe (sHX32; JEOL RESONANCE, Japan) was used for solid-state NMR. The sample was placed into a 3.2 mmφ zirconium rotor with

a vespel cap and cross-polarization and magic angle spinning (CP/MAS) NMR spectra were acquired with high-power ^{1}H decoupling at an MAS frequency of 15 kHz at an inlet air temperature of ambient temperature. The relaxation delay was set based on the ^{1}H spin lattice relaxation time of each sample, which was predetermined using the saturation recovery method. The CP contact time was set at 5 ms. The ^{13}C spectra were externally referenced by setting the methyl peak of hexamethylbenzene to 17.2 ppm. The ^{15}N spectra were externally referenced by setting the ammonium peak of ammonium chloride to 39.3 ppm. A 5.0 mm FG/AT probe (RO5AT; JEOL RESONANCE) was used for solution NMR. The samples were placed into a 5.0 mmφ glass tube and the NMR spectra were obtained at an inlet air temperature of 25 °C. GA solution was prepared by dissolving 50 mg of GA into 2 mL of 0.15 mol/L HCl solution. Sodium gentisate solution was prepared by dissolving 50 mg of gentisic acid into 1 mL of 0.48 mol/L NaOH solution. Both solutions contained 40% (v/v) D_2O and 0.1% (w/v) TSP-d_4 to provide a signal for the magnetic field frequency lock and internal chemical shift standard.

2.11. Single-Crystal X-Ray Diffraction (SCXRD)

SCXRD data were collected at −173 °C using XtaLAB P200 (Rigaku Corporation, Tokyo, Japan) with Cu-Kα radiation generated at 40 kV/30 mA. The crystal structures were solved by direct methods and refined by a full-matrix least-squares procedure. The N–H and O–H hydrogen atoms were refined isotropically from the difference Fourier map. The non-hydrogen atoms were refined anisotropically. The hydrogen atoms were located geometrically and refined using the riding model. All calculations were performed using the CrystalStructure11 crystallographic software package, except for refinement, which was performed using SHELXL [32].

2.12. Formulation Preparation for PK Study

Immediate release (IR) tablets (300 mg of TAK-020) were prepared by combining D-mannitol, microcrystalline cellulose, HPC, Primojel®, and magnesium stearate. TAK-020/GA CC (100 mg of TAK-020) was prepared by encapsulation in a gelatin capsule. The HPMCP HP-55 polymer and TAK-020 were dissolved in DMSO/TFE at 20% loading as the TAK-020 weight ratio and ASD was obtained by lyophilization. Subsequently, ASD tablets (100 mg of TAK-020) were prepared by mixing D-mannitol, microcrystalline cellulose, AcDisol®, Aerosil®, and magnesium stearate with ASD. Nanocry suspension (ca. 200 nm diameter) was made by the wet milling method, as previously described [10]. TAK-020 suspension containing HPC and docusate sodium was wet-milled with zirconia beads (0.1 mm diameter) in a NP-100 rotation/revolution nano pulverizer (Thinky Co., Ltd., Tokyo, Japan). LBF was made by dissolving TAK-020 in corn oil and Capmul® MCM C8.

2.13. In Vivo PK Study

All studies involving dogs were approved by the Institutional Animal Care and Use Committee of Takeda Pharmaceutical Company. The male beagle dogs were treated to regulate normal intragastric pH via pentagastrin administration 15 min before administration. IR tablet, TAK-020/GA CC, Nanocry, ASD, and LBF were orally administered to fasted dogs, and blood samples were collected 0.25, 0.5, 1, 2, 4, 6, 8, 12, and 24 h later. Blood samples were mixed with 100 µL of ACN, 10 µL of internal standard, and 10 µL of mobile phase—purified water/ACN/formic acid (600:200:0.1, v/v/v); and the plasma was extracted by centrifuging for 3 min at 1600 × *g* at ambient temperature. The supernatant was diluted 3-fold using purified water/formic acid (1000:0.1, v/v/v) and subjected to centrifugation for 1 min at 1600 × *g* at ambient temperature. The resulting supernatant was analyzed by liquid chromatography tandem mass spectrometry (LC−MS/MS) as follows (Section 2.14). The C_{max} and T_{max} were taken from the actual values and the $AUC_{0–24\,h}$ was calculated by the trapezoidal method.

2.14. LC−MS/MS

LC−MS/MS quantification was carried out using LC−10ADvp series (Shimadzu Corporation, Kyoto, Japan) and API5000 mass spectrometer (AB Scientific Export, Massachusetts, USA).

The separation of the analytes used a Kinetex C18 column (50 mm × 2.0 mm I.D., 2.6 µm; Phenomenex, California, USA) at 40 °C and purified water/ACN/formic acid (600:200:0.1, v/v/v) as the mobile phase. The flow rate was 0.2 mL/min; 20 µL of the plasma sample in supernatant was injected into LC−MS/MS; and the running time for one injection was 5 min. The mass spectrometer was operated in the positive electrospray ionization mode. Analyst®Software was used for data acquisition and processing. TAK-020 was monitored using selective reaction monitoring method with transitions of m/z 352.4→124.1.

2.15. Statistics

Statistical analyses for multiple comparisons were performed by analysis of variance (two-way ANOVA) followed by the Student–Newman–Keuls test or Bonferroni analysis. Results with $p < 0.01$ or $p < 0.05$ were considered to be statistically significant.

3. Results and Discussion

3.1. Preparation of TAK-020 Cocrystals with Three Types of Screening

As a result of cocrystal screenings determined by PXRD, seven types of probable TAK-020 cocrystal (TAK-020 with CA, MoA, MeA, MaA, MdA, GA, and SA) were obtained in CCG and SCS (Tables 1 and 2, and Figure 1) [33]. The PXRD patterns of each scale-up powder exhibited differences from TAK-020 and their individual CCFs (Figures 2 and A1), and were consistent with the screening results. In terms of the thermal behavior, TAK-020 shows only an exotherm at 300 °C (Figure 3(Ba)) and individual CCFs show sharp endothermic peaks within ca. 200°C (Figure A2). On the other hand, their new forms exhibited complex and unique endothermic peaks with no significant weight loss until melting on TG curves (Figure 3A). The observed endothermic peaks at lower temperatures among some forms might represent the eutectic melting of residual CCF and other things, and they were different from those of individual CCFs, suggesting that their unique endothermic peaks might show melting points of new crystal complex. Furthermore, stepwise weight loss was shown, and that was involved in the decomposition of CCF, followed by the melting of crystal structure. (Figures 3 and A2). The results of thermal analysis supported the determination of formed TAK-020 anhydrous cocrystal as a complex crystal. Obtained crystals were determined as TAK-020 cocrystals from combined factors of new PXRD patterns, their thermal behavior, and the pKa values of the CCFs used. Consequently, cocrystal screenings found the seven novel cocrystals of TAK-020.

Table 1. Results of TAK-020 cocrystal screening.

CCF	CRC	CCG	SCS	CCF	CRC	CCG	SCS
Citric acid (CA)	-	✓	✓	Lactamide		-	
Fumaric acid	-	-	-	Glycolamide		-	
Glutaric acid (GA)		-		Tromethamine		-	-
Malonic acid (MoA)	-	✓	✓	Meglumine	-	-	-
Succinic acid	-	-	-	Glycine		(-)	
Maleic acid (MeA)	-	✓	✓	L-Arginine	-	(-)	-
L-Malic acid (MaA)		✓	✓	L-Lysine	-	(-)	-
L-Tartaric acid	-	-	-	L-Proline		(-)	
Mandelic acid			✓	L-Tryptophan		(-)	
Benzoic acid	-	-	-	Phosphoric acid		-	
Gentisic acid (GA)	-	✓	✓	L-Ascorbic acid		-	
Salicylic acid (SA)	-	✓	✓	Urea	-	-	-
Hippuric acid	-	-	-	Saccharin	-	-	-
Nicotinamide	-	-	-	Ethylmaltol		-	-
Benzamide		-					

Conventional reaction crystallization (CRC); cocktail cocrystal grinding (CCG); saturated CCF solution slurry (SCS); ✓, new form; -, free and/or cocrystal former (CCF); (-), amorphous or low crystallinity; empty, not tested.

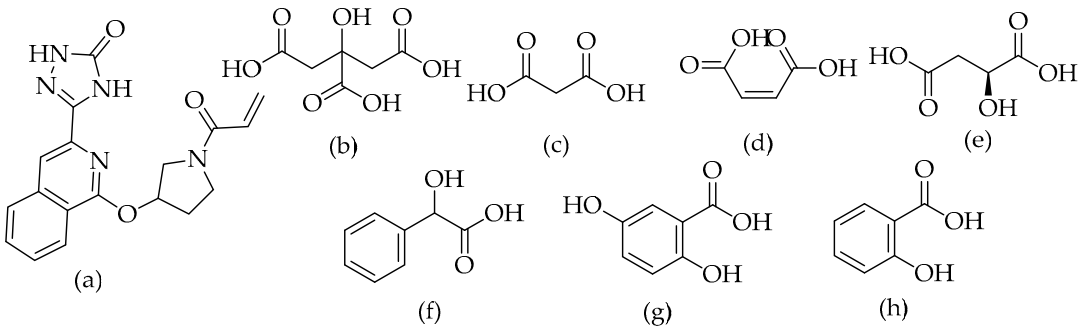


Figure 1. Chemical structures of (**a**) TAK-020, (**b**) citric acid (CA), (**c**) malonic acid (MoA), (**d**) maleic acid (MeA), (**e**) L-malic acid (MaA), (**f**) mandelic acid (MdA), (**g**) gentisic acid (GA), and (**h**) salicylic acid (SA).

Table 2. Physicochemical properties of CCFs co-crystallized with TAK-020.

CCF Group	CCF Name	Molecular Weight (Da)	H-Acceptor	H-Donor	pKa
Tri-carboxylic acid	Citric acid	192	7	4	3.1, 4.8, 6.4
Di-carboxylic acid	Malonic acid	104	2	4	2.8, 5.7
	Maleic acid	116	4	2	1.9, 6.2
	L-Malic acid	134	5	3	3.5, 5.1
Aromatic and carboxylic acid	Mandelic acid	152	3	2	3.4
	Gentisic acid	154	4	3	2.9
	Salicylic acid	138	3	2	3.0, 13.8

Physicochemical properties are quoted from the literature [20,29].

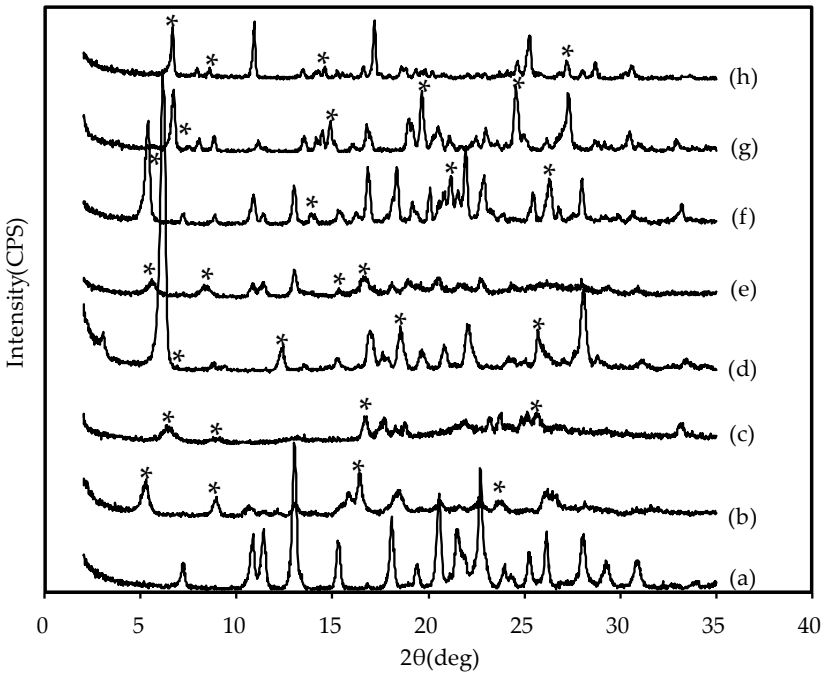


Figure 2. Powder X-ray diffractometry (PXRD) patterns of (**a**) TAK-020, (**b**) TAK-020/CA, (**c**) TAK-020/MoA, (**d**) TAK-020/MeA, (**e**) TAK-020/MaA, (**f**) TAK-020/MdA, (**g**) TAK-020/GA, and (**h**) TAK-020/SA. * Main distinctive peaks different form TAK-020 and the corresponding CCFs.

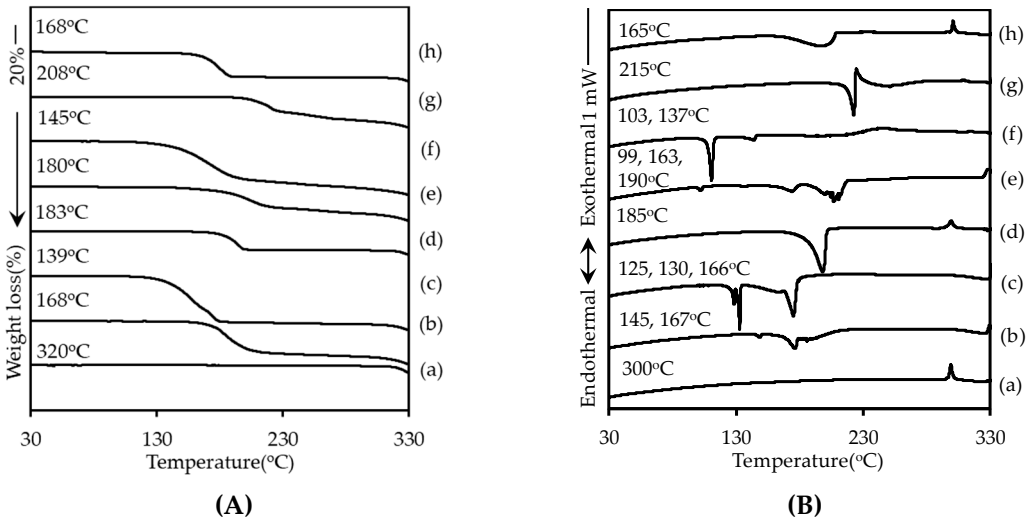


Figure 3. (**A**) Thermogravimetry (TG) and (**B**) differential scanning calorimetry (DSC) curves of (**a**) TAK-020, (**b**) TAK-020/CA, (**c**) TAK-020/MoA, (**d**) TAK-020/MeA, (**e**) TAK-020/MaA, (**f**) TAK-020/MdA, (**g**) TAK-020/GA, and (**h**) TAK-020/SA. Starting temperatures at weight loss are shown on the left side in the TG curve. Endothermal temperatures are shown on the left side in the DSC curve.

Regarding the three types of screening, cocrystals of TAK-020 were found on CCG and SCS, but not CRC. Since SCS and CRC are same solution-based screening methods, their difference would be likely due to the different statuses of saturated concentration for APIs and CCFs, which can be followed by solubility product (Ksp) [14]. SCS suspended API into a saturated CCF solution, and this method gave the status of saturated concentration for both API and CCFs in crystallization solvent, which would promote cocrystal formation followed by Ksp. On the other hand, as for CRC, since either the dissolving amount of API or CCF was low and far from saturated concentration in crystallization solvents, cocrystal formation would not be preferentially promoted. In addition, as for CCG screening, since this method is a solid-state screening, there is no need to consider a Ksp and a component–solvent interaction contrary to solution-based screening methods as advantageous. This method reduce crystallinity and promote amorphization, so there is a possibility to discover not only a cocrystal but also a coamorphous. However, taken together, to discover new types of cocrystals, multi-faceted screenings such as solution or solid-based methods would be useful.

Non-structural correlations (molecular weight, and the numbers of H-donors and H-acceptors) of the CCFs being able to generate the novel cocrystals or not were obtained, but these CCFs which generated cocrystals have a carboxy group and/or a hydroxy group (Tables 1 and 2, and Figure 1). However, even the other CCFs for which a cocrystal was not formed were shown to have a carboxy group and/or a hydroxy group in the screening. It is inferred that cocrystal packing is not formed due to the individuality or complexity of a crystal's intermolecular interactions, packing energy, and three-dimensional structure regarding the interaction site. From the cocrystal-formed CCFs, the carboxy group and/or the hydroxy group might be the key groups for intermolecular interaction with TAK-020 in a cocrystal.

3.2. In Vitro Dissolution Performance for Selecting Cocrystal Form

Dissolution and IDR were determined to evaluate cocrystal effectiveness and to choose the best cocrystal form in terms of enhanced dissolution and solubility. Dissolution as a short-term evaluation using bile acid, would be appropriate for assessing the dissolution capacities and absorbencies to avoid the cocrystal dissociation risk due to a closed system, unlike in vivo [14,34]. Regarding the results of dissolution evaluation, dissolved amounts of all cocrystals exceeded those of TAK-020 free; the ratio of enhancement was approximately 1.2–9.4 times in aqueous solutions of JP1 and JP2, and approximately

2.0–5.9 times in biorelevant solutions of FaSSIF and FeSSIF (Table 3). Notably, a significant difference of enhanced dissolution was observed in bile acid on all cocrystals. Even though some cocrystals exhibited no significant difference of enhanced dissolution in aqueous solutions of JP1 and JP2, all cocrystals would be expected to contribute to improved absorption via the oral route.

Table 3. Dissolution of TAK-020 in aqueous and biorelevant test solutions at 37 °C for 2 h.

Media	Dissolved Amount as TAK-020 (μg/mL)											
	JP1 (pH 1.2)			JP2 (pH 6.8)			FaSSIF (pH 6.5)			FeSSIF (pH 5.0)		
TAK-020	1.6	±	0.0	1.7	±	0.1	3.0	±	0.9	10.4	±	0.2
TAK-020/CA CC	1.9	±	0.1	2.2	±	0.0	7.3	±	0.3**	30.4	±	0.4**
TAK-020/MoA CC	7.2	±	1.0**	15.9	±	1.2**	10.0	±	0.3**	36.0	±	5.0**
TAK-020/MeA CC	2.4	±	0.4	5.7	±	0.2**	9.5	±	0.9**	25.9	±	0.4**
TAK-020/MaA CC	2.1	±	0.0	5.6	±	0.4**	8.6	±	0.2**	29.2	±	1.8**
TAK-020/MdA CC	2.4	±	0.3	5.0	±	0.4**	8.1	±	0.3**	27.3	±	0.7**
TAK-020/GA CC	7.4	±	0.3**	2.8	±	0.6	9.4	±	0.4**	27.1	±	1.2**
TAK-020/SA CC	9.3	±	1.0**	3.8	±	0.6*	17.8	±	0.9**	21.1	±	1.1**

Cocrystal (CC); Japanese Pharmacopoeia disintegration 1st and 2nd test fluid (JP1, pH 1.2), JP2 (pH 6.8); fasted state simulated intestinal fluid version 2 (FaSSIF); fed state simulated intestinal fluid (FeSSIF); mean ± standard deviation ($n = 3$), p-value vs. TAK-020 free form ($p < 0.01^{**}$, $p < 0.05^{*}$).

Although the dissolution test at one time is useful to verify the effect of cocrystals on the enhanced solubility, it is only the result of a temporary point passing through an unclear dissolved-amount curve, such as dissolution, saturation, sustained supersaturation, and decline from instantaneous dissolving. It does not lead to a definitive comparison among cocrystals. Hence, IDR profiles of cocrystals excluding particle diffusion were evaluated for the selection of the most effective cocrystal. IDR is proportional to solubility in test solutions, and the dissolution rate per constant surface area could be evaluated, which could rule out the impacts of particle size and diffusion. There was clear linearity of all IDR profiles, with an R^2 value of 0.94–1.00 up to 10 min; all IDRs of cocrystals were increased in comparison with that of TAK-020 free form, as was the case for the dissolution results (Figure 4). The IDRs of TAK-020/MeA, GA, and SA CCs were 54, 47, and 52 times higher than for TAK-020 free for 30 min, respectively. These three cocrystals thus enhanced solubility and were selected as developed cocrystal candidates that could significantly impact in vivo exposure.

The highest-performing cocrystal should be selected to develop a solid form, but information on the toxicity and actual use for marketed drugs has to be taken into account for CCF selection. MeA is widely used as a salt counter acid for marketed drugs [29], whereas GA and SA have no practical use for drugs as counter acids, only being used in research, as reported in the literature [24]. In terms of CCF toxicity, SA is reported to irritate gastrointestinal intestinal mucosa and other tissues. The maximum daily intake of MeA, 250 mg, exists for the administration of acetophenazine hydrogenmaleate, but acute tubular necrosis in dogs, severe irritation to the mucous membranes in humans, and alterations in the physical states of human erythrocyte membrane proteins in vitro are concerning [29,35]. GA is a metabolite of aspirin in the liver and has been applied as an additive for octreoscan injection, which is approved by the FDA [36]. It is also known to be present as a normal constituent of serum [37] and in foods, including cereals, such as wheat and rye, herbs, mushrooms, and a variety of fruits and beverages [38–40]. In other words, the tolerability of GA is higher than those of SA and MeA.

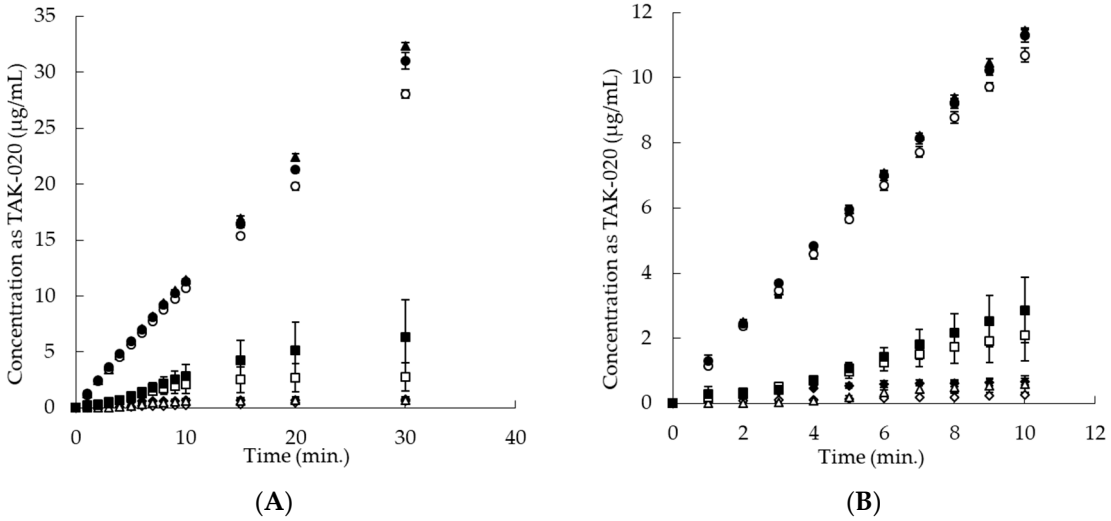


Figure 4. Profiles of intrinsic dissolution rate in JP2 (pH 6.8) containing 200 mM sodium cholate at 37 °C for (**A**) 30 min and (**B**) initial dissolution rate up to 10 min. (◇) TAK-020, (◆) TAK-020/CA CC, (△) TAK-020/MoA CC, (▲) TAK-020/MeA CC, (□) TAK-020/MaA CC, (■) TAK-020/MdA CC, (○) TAK-020/GA CC, (●) TAK-020/SA CC (n = 3).

Besides, the dissociation profiles of TAK-020/GA CC were evaluated using μFLUX™, which is an in vitro absorption potential measurement system mimicking the human gastrointestinal tract, to determine cocrystal dissociation prior to the API absorption reaching the site of action (Figure 5). GA from the cocrystal completely dissolved in the donor chamber—this was the dissolution behavior within 1 h, whereas TAK-020 was slightly dissolved, suggesting cocrystal dissociation before absorption. In contrast, GA permeated into the receiver chamber, mimicking blood circulation at a much lower rate than TAK-020. It was indicated that the cocrystal dissociated before absorption and substantial absorption of GA did not occur. Accordingly, the safety margin of GA would be sufficiently secured in the TAK-020 drug dosage range and there is room for selecting GA as a CCF based on this.

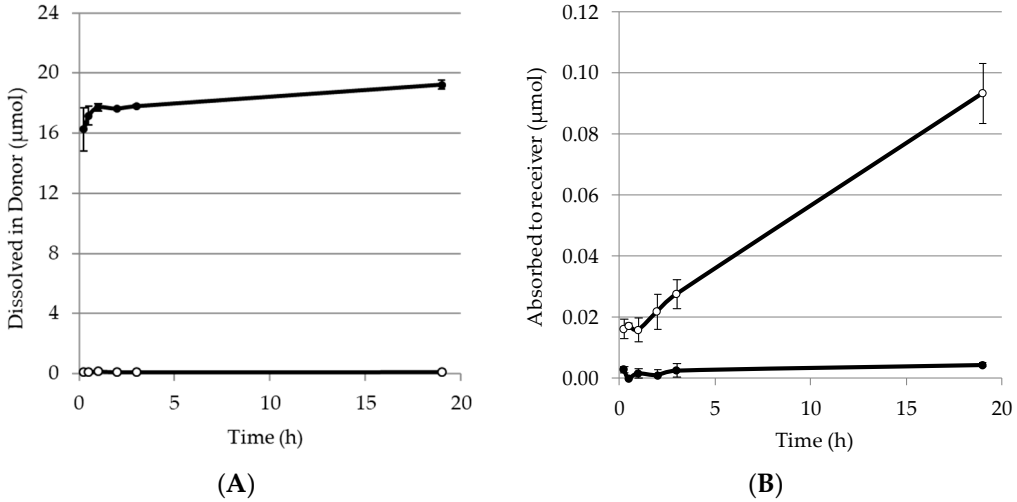


Figure 5. (**A**) Profiles of dissolution in the donor chamber and (**B**) absorption in the receiver chamber of TAK-020, and GA in a combination test with transmembrane permeation at 37 °C. Initial nominal calculated amount of TAK-020 and GA was 18.2 μmol. (○) TAK-020 and (●) GA (n = 3).

3.3. Certification of the Cocrystal Definition

TAK-020/GA CC has to be proven to be in a specific stoichiometric ratio and to undergo non-ionic interactions, thereby definitively classifying it as a cocrystal, in accordance with regulatory guidelines

ensuring cocrystal performance. Hence, the pKa values of TAK-020 and GA were confirmed by a simple approach to categorize non-ionic interactions (Figure 6). The basic pKa at the isoquinoline position of TAK-020 and the acidic pKa at the carboxyl position of GA were calculated as 2.33 and 2.05, respectively, using ACD Labs version 12.01; the reported experimental value of the GA acidic pKa is 2.95 [41]. ΔpKa [pKa (base) − pKa (acid))] values were derived as 0.28 and −0.62, respectively. Since substantial proton transfer would not occur in cases where ΔpKa is 1 or less, the resultant ΔpKa was indicated to be a cocrystal.

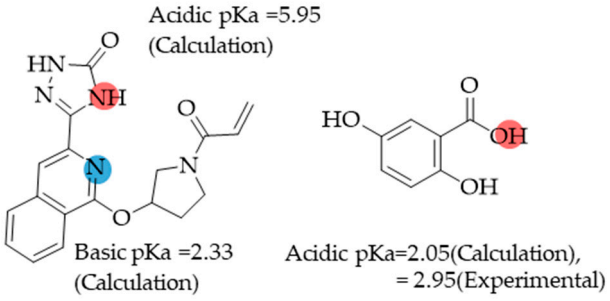


Figure 6. pKas of TAK-020 and GA.

NMR is useful for obtaining experimental proof of a non-protonated state at the molecular level. If a complex crystal is formed by the ionic bonding of salt formation, ^{13}C and ^{15}N peaks related to the interaction typically shift. Thus, the molecular state is inferred from the chemical shift by relative comparison of reference peaks with ionized and neutral states [42,43]. ^{15}N chemical shift in the isoquinoline ring was not observed between TAK-020/GA CC and TAK-020, indicating that N5 is not protonated for ion binding due to salt formation in a complex crystal of TAK-020 and GA. In contrast, different ^{15}N chemical shifts for the triazolone of N12 and pyrrolidine of N22 were revealed from local environmental changes. It is possible that this is related to the site of interaction with GA or intermolecular interaction of crystal lattice (Figure 7). ^{13}C CP/MAS NMR spectra of the carboxyl C=O peak in GA represent the molecular state, and ionized and neutral states were clearly identified. However, the ^{13}C chemical shift of the carboxyl group in TAK-020/GA CC was observed at a higher magnetic field than that of the neutral state in GA solution at pH 1.2, and it did not completely shift to the ionized state. The protonation of GA in TAK-020/GA CC was also ruled out (Figure 8). This provided experimental support that TAK-020/GA CC features non-ionic interactions.

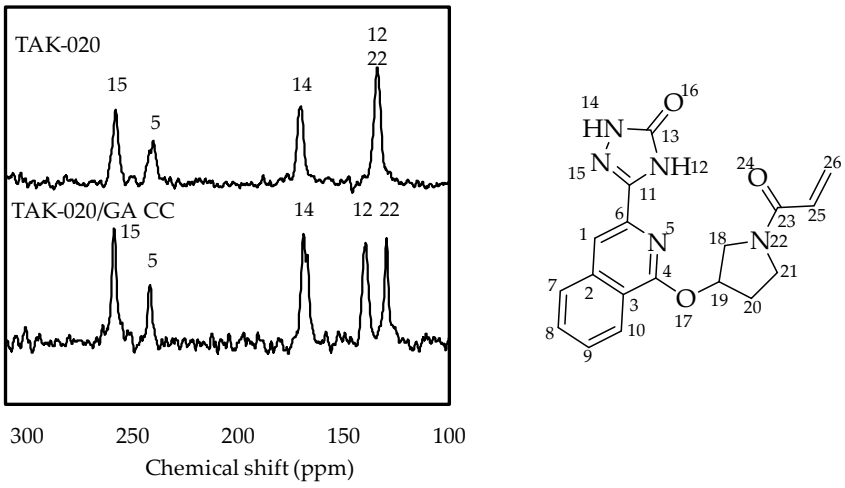


Figure 7. ^{15}N nuclear magnetic resonance (NMR) spectra.

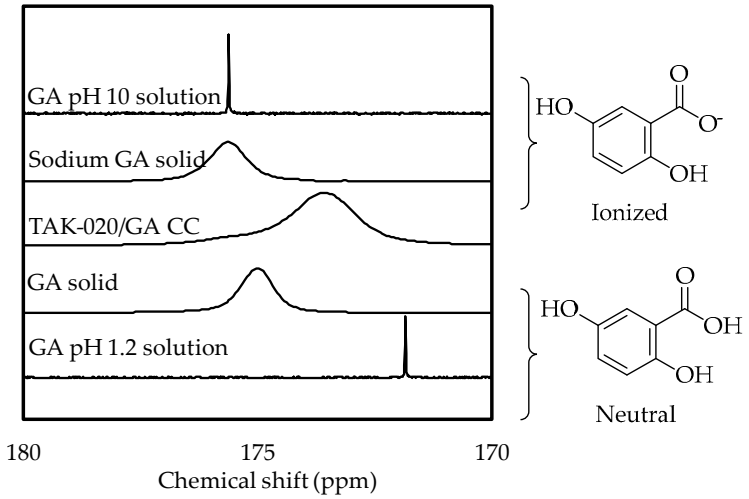


Figure 8. ^{13}C CP-MAS NMR spectra of the carboxyl group.

The crystal structure of TAK-020/GA CC was also acquired by SCXRD. It provides a rational basis for its status as a cocrystal, based on the specific stoichiometric ratio and the binding site of TAK-020 and GA—found through matching of experimental and calculated PXRD patterns. The acquired crystal structure of TAK-020/GA CC exhibited one-to-one complexes and two sets of the complex molecules TAK-020/GA CC had determinate stoichiometric ratios. It also revealed interacting functional moieties between triazolone nitrogen and oxygen of TAK-020 and carboxylic acid oxygen and hydrogen of GA, the distance between which allowed the possibility of hydrogen bonds forming. Furthermore, the C–O and C=O bond length ratio of the carboxylic group in GA was 1.044, which indicated that protonation had not occurred for complex binding [31,44] (Table 4 and Figure 9). From a series of analyses, TAK-020/GA CC has been clearly proven to be a cocrystal, in line with regulatory guidelines.

Table 4. Crystallographic data of TAK-020/GA CC.

Molecular Formula	**$C_{25}H_{23}N_5O_7$**
Molecular weight	505.49
Temperature (K)	100
Crystal dimensions (mm)	0.050 × 0.010 × 0.002
Crystal system	Monoclinic
Space group	$P2_1$ (#4)
a (Å)	13.6572
b (Å)	19.8263
c (Å)	8.9035
α (°)	(90)
β (°)	105.883
γ (°)	(90)
V (Å^3)	2318.8
Z	4
Calculated density (g/cm^3)	1.448
R (I > 2.00 σ (I))	0.0905
R_w	0.2649

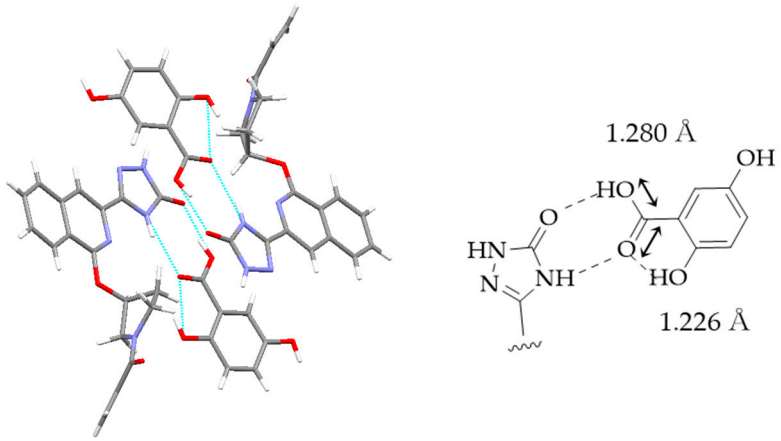


Figure 9. Crystal packing diagram of TAK-020/GA CC including the H-bonding motifs and the interaction motif showing the C–O bond lengths between triazolone of TAK-020 and carboxylic acid of GA.

3.4. PK Profiling for Determining the Optimal Drug Form

TAK-020/GA CC is a viable candidate to improve bioavailability, leading to reliable pharma-cological efficacy from the enhanced dissolution. However, drug products have to be selected from all candidates of oral form and formulation, including solubilized formulations with the potential for development. Hence, dog PK studies were carried out to find the optimal candidate using TAK-020/GA CC as crystal engineering technology and solubilized formulations of ASD, Nanocry, and LBF. An IR tablet was orally administered as a negative control for comparison. The average plasma concentration and profile in dog PK studies are summarized in Figure 10 and Table 5.

Better absorption profiles were achieved in the order TAK-020/GA CC, ASD, Nanocry, LBF, and IR based on $AUC_{0–24h}$. Interestingly, TAK-020/GA CC resulted in exceeding the $AUC_{0–24h}$ of the known solubilized formulation and TAK-020/GA CC showed significantly higher $AUC_{0–24h}$ than the IR tablet (negative control) using TAK-020 micronized crystalline. The enhanced absorption of TAK-020/GA CC reached approximately 60-fold $AUC_{0–24h}$ compared with dose-corrected IR tablet. With a trend of enhanced in vivo and in vitro ratios, IDR correlated better with the enhanced absorption than the dissolution. Inferences were made about the reasons for the effects of particle diffusion, evaluation time, test concentration, and rate limiting step in vivo. Since these in vitro assessments do not include the elimination of dissolved API by absorption that occurs in vivo, it would be desirable for cocrystal capability profiling related to in vivo absorption to approach closer to sink conditions by evaluation using biorelevant media at low concentrations in a short time, in the case of closed conditions in vitro.

The selection of the best technology for enhanced absorption is related to numerous factors and variables reflecting the physicochemical properties, such as Log P and melting point, as supportive tools for formulation selection. In particular, API with a high melting point has a strong crystallization tendency, which is not suitable for ASD [7], and intestinal lymphatic transport of API on LBF is not even expected at low lipophilicity, log P < 5 [45]. TAK-020 exhibits an exotherm at high temperatures of around 300 °C, including melting, and it has relatively low lipophilicity (cLogP 2.0 calculated by Daylight version 4.95). It is likely that the physicochemical properties of TAK-020 have not realized the formulation performance of ASD and LBF. Nanocry improves the dissolution rate owing to increased surface area by particle size reduction, but it was not adequate for TAK-020, whose solubility would be the rate limiting factor. CCF solubility, which is much higher than that of API, leads to the cocrystal being more soluble than API [14]. It is suggested that cocrystals modify the maximum degree of API solubility, even in the gastrointestinal tract. As a result, TAK-020/GA CC was presented to be superior to the solubilized formulations in a variety of functional types, and the cocrystal proved to be the best solid form for TAK-020 regarding translational development of an oral form.

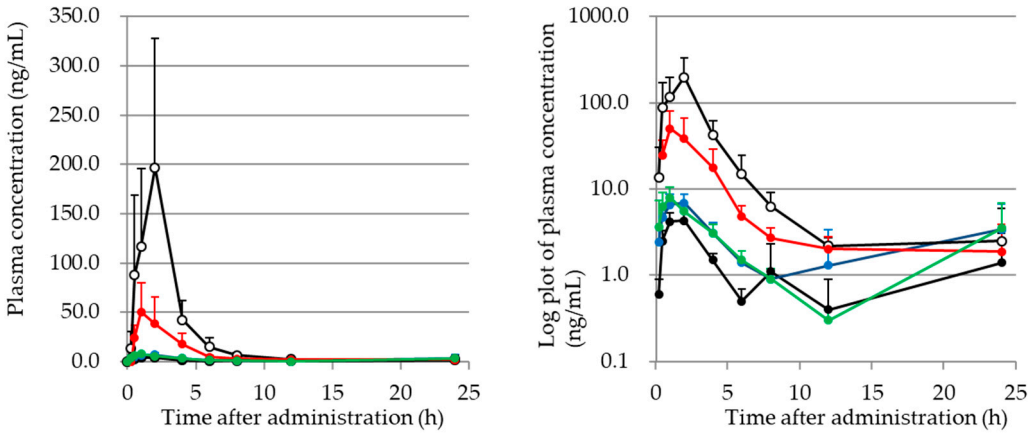


Figure 10. (**A**) Plasma concentration and (**B**) log plot of plasma concentration in dogs after oral administration. (●) Immediate release (IR) tablet, (○) TAK-020/GA CC, (●) amorphous solid dispersion (ASD) tablet, (●) nanocrystal (Nanocry) suspension, (●) lipid-based formulation (LBF) (n = 4–5).

Table 5. Pharmacokinetic parameters after oral administration of each formulation.

Formulation	Dose (mg)	T_{max} (h)			C_{max} (ng/mL)			$AUC_{0–24\ h}$ (ng·h/mL)		
IR tablet	300	1.6	±	0.5	4.7	±	1.0	30.2	±	14.5
TAK-020/GA CC	100	1.3	±	0.7	229.0	±	106.5**	585.6	±	231.5**
ASD tablet	100	0.4	±	0.1	51.5	±	29.8	130.2	±	88.3
Nanocry suspension	100	1.4	±	0.5	7.7	±	1.8	59.6	±	31.8
LBF	100	5.6	±	10.3	8.3	±	2.0	52.6	±	20.8

Mean ± standard deviation (n = 4–5), p-value vs. 300 mg IR tablet ($p < 0.01^{**}$, $p < 0.05^{*}$).

4. Conclusions

The cocrystals of TAK-020 were successful, with CCFs having a carboxy group, as revealed by cocrystal screenings of slurry aging and grinding based on crystal engineering theory. These cocrystals were superior to the free form in terms of dissolution and solubility. TAK-020/GA CC selected by in vitro performance exhibited the best absorption in dog PK studies among the various solubilized formulation techniques. The cocrystal presented the exceeding case of current existing solubilized formulations depending on its physicochemical properties. The results demonstrate the attractiveness of cocrystals for pharmaceutical development.

TAK-020/GA CC has a specific stoichiometric ratio and non-ionic interactions between TAK-020 and GA, as revealed by the pKa difference, solid-state NMR, and single X-ray structure analysis. The development of cocrystals is being accelerated with recent regulatory developments, and cocrystal development can be further promoted by developing reliable analytical techniques appropriate to the regulations. Furthermore, the developmental form of a pharmaceutical product must consider the patient's quality of life, and development difficulties, such as manufacturing cost and timeline-related pharmaceutical development. Cocrystals can be an acceptable drug product of regular tableted formulation and manufactured in general facilities; a normal tablet size leads to easy intake and is desirable for patients. Taking these factors into consideration, it is worthwhile developing TAK-020/GA CC as the translational solid form.

In conclusion, we determined TAK-020/GA CC to be the most optimal solid form having enhanced oral absorption from a series of studies. TAK-020/GA CC was definitively defined as a cocrystal in line with the guidelines. We expect that clinical trial and drug development for it will proceed steadily, for general solid forms of salt or free crystal.

Author Contributions: Conceptualization, K.Y. and K.K.; formal analysis and investigation, K.K., M.Y., M.K., M.H., and J.T.; writing—original draft preparation, K.K.; writing—review and editing, M.Y., M.K., and Y.I.; visualization, K.K.; supervision, M.K, K.Y., and Y.I.; project administration, K.K. and M.Y. All authors have read and agreed to the published version of the manuscript.

Funding: This research received no external funding.

Acknowledgments: We are deeply grateful to colleagues of Pharmaceutics Research Shonan in Analytical Development in Takeda Pharmaceutical Company Limited for discussions and support. Special thanks also go to Masato Kitayama currently of Spera Pharma, Inc., formerly of Pharmaceutics Research in Process Chemistry in Takeda Pharmaceutical Company Limited for the synthesis and supply of the drug substance and cocrystal.

Conflicts of Interest: The authors declare no conflict of interest.

Appendix A

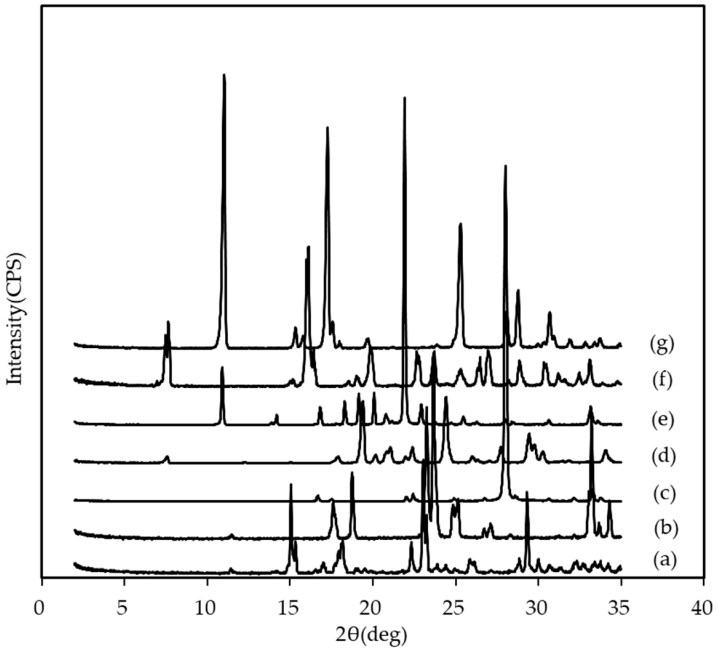


Figure A1. PXRD patterns of (**a**) CA, (**b**) MoA, (**c**) MeA, (**d**) MaA, (**e**) MdA, (**f**) GA, and (**g**) SA.

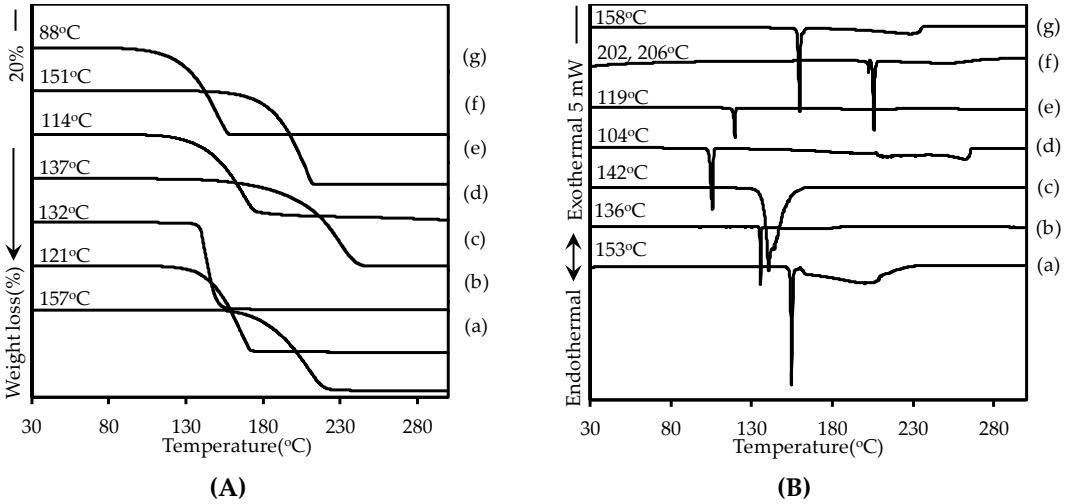


Figure A2. (**A**) TG and (**B**) DSC curves of (**a**) CA, (**b**) MoA, (**c**) MeA, (**d**) MaA, (**e**) MdA, (**f**) GA, and (**g**) SA. Starting temperatures at weight loss are shown on the left side in the TG curve. Endothermal temperatures are shown on the left side in the DSC curve.

References

1. Nakashima, S.; Yamamoto, K.; Arai, Y.; Ikeda, Y. Impact of physicochemical profiling for rational approach on drug discovery. *Chem. Pharm. Bull.* **2013**, *61*, 1228–1238. [CrossRef] [PubMed]
2. Benet, L.Z.; Broccatelli, F.; Oprea, T.I. BDDCS applied to over 900 drugs. *AAPS J.* **2011**, *13*, 519–547. [CrossRef] [PubMed]
3. Takagi, T.; Ramachandran, C.; Bermejo, M.; Yamashita, S.; Yu, L.X.; Amidon, G.L. A provisional biopharmaceutical classification of the top 200 oral drug products in the United States, Great Britain, Spain, and Japan. *Mol. Pharm.* **2006**, *3*, 631–643. [CrossRef] [PubMed]
4. Vinod, P.; Sunil, P.; Sonali, P.; Tejaswini, P.; Sachinkumar, P.; Shitalkumar, P. Solubility enhancement of poorly soluble drugs by using novel techniques: A review. *J. Curr. Pharm. Res.* **2014**, *4*, 1258–1270.
5. Blagden, N.; Matas, M.D.; Gavan, P.T.; York, P. Crystal engineering of active pharmaceutical ingredients to improve solubility and dissolution rates. *Adv. Drug. Deliv. Rev.* **2007**, *59*, 617–630. [CrossRef] [PubMed]
6. Prohotsky, D.; Zhao, F. A survey of top 200 drugs inconsistent practice of drug strength expression for drugs containing salt forms. *J. Pharm. Sci.* **2012**, *101*, 1–6. [CrossRef]
7. Fridgeirsdottir, G.A.; Harris, R.; Fischer, P.M.; Roberts, C.J. Support tools in formulation development for poorly soluble drugs. *J. Pharm. Sci.* **2016**, *105*, 2260–2269. [CrossRef]
8. Zhu, B.; Zhang, Q.; Wang, J.; Mei, X. Cocrystals of baicalein with higher solubility and enhanced bioavailability. *Cryst. Growth Des.* **2017**, *17*, 1893–1901. [CrossRef]
9. Yamamoto, K.; Kojima, T.; Karashima, M.; Ikeda, Y. Physicochemical evaluation and developability assessment of coamorphouses of low soluble drugs and comparison to the co-crystals. *Chem. Pharm. Bull.* **2016**, *64*, 1739–1746. [CrossRef]
10. Karashima, M.; Kimoto, K.; Yamamoto, K.; Kojima, T.; Ikeda, Y. A novel solubilization technique for poorly soluble drugs through the integration of nanocrystal and cocrystal technologies. *Eur. J. Pharm. Sci.* **2016**, *107*, 142–150. [CrossRef]
11. Aakeröy, C.B.; Salmon, D.J. Building co-crystals with molecular sense and supramolecular sensibility. *Cryst. Eng. Comm.* **2005**, *7*, 439–448. [CrossRef]
12. Shan, N.; Zaworotko, M.J. The role of cocrystals in pharmaceutical science. *Drug Discov. Today* **2008**, *13*, 440–446. [CrossRef] [PubMed]
13. Schlutheiss, N.; Newman, A. Pharmaceutical cocrystals and their physicochemical properties. *Cryst. Growth. Des.* **2009**, *9*, 2950–2967. [CrossRef] [PubMed]
14. Good, D.J.; Rodríguez-Hornedo, N. Solubility advantage of pharmaceutical cocrystals. *Cryst. Growth Des.* **2009**, *9*, 2252–2264. [CrossRef]
15. ter Horst, J.H.; Deij, M.A.; Cains, P.W. Discovering new co-crystals. *Cryst. Growth Des.* **2009**, *9*, 1531–1537. [CrossRef]
16. Malamatari, M.; Ross, S.A.; Douroumis, D.; Velaga, S.P. Experimental cocrystal screening and solution based scale-up cocrystallization methods. *Adv. Drug. Deliv. Rev.* **2017**, *117*, 162–177. [CrossRef]
17. Leung, D.H.; Lohani, S.; Ball, R.G.; Canfield, N.; Wang, Y.; Rhodes, T.; Bak, A. Two novel pharmaceutical cocrystals of a development compound –screening, scale-up, and characterization. *Cryst. Growth Des.* **2012**, *12*, 1254–1262. [CrossRef]
18. Meanwell, N.A. The emerging utility of co-crystals in drug discovery and development. *Annu. Rep. Med. Chem.* **2008**, *43*, 373–401.
19. Kojima, T.; Tsutsumi, S.; Yamamoto, K.; Ikeda, Y.; Moriwaki, T. High-throughput cocrystal slurry screening by use of in situ Raman microscopy. *Int. J. Pharm* **2010**, *399*, 52–59. [CrossRef]
20. Yamamoto, K.; Tsutsumi, S.; Ikeda, Y. Establishment of cocrystal cocktail grinding method for rational screening of pharmaceutical cocrystals. *Int. J. Pharm* **2012**, *437*, 162–171. [CrossRef]
21. Yamashita, H.; Hirakura, Y.; Yuda, M.; Teramura, T.; Terada, K. Detection of cocrystal formation based on binary phase diagrams using thermal analysis. *Pharm. Res.* **2013**, *30*, 70–80. [CrossRef]
22. US Food and Drug Administration. Regulatory classification of pharmaceutical co-crystals guidance for industry. Available online: https://www.fda.gov/regulatory-information/search-fda-guidance-documents/regulatory-classification-pharmaceutical-co-crystals (accessed on 27 January 2020).

23. European Medicines Agency. Reflection paper on the use of cocrystals and other solid state forms of active substances in medicinal products. Available online: https://www.ema.europa.eu/en/use-cocrystals-active-substances-medicinal-products#current-version-section (accessed on 27 January 2020).
24. Gadade, D.D.; Pekamwar, S.S. Pharmaceutical cocrystals: Regulatory and strategic aspects, design and development. *Adv. Pharm. Bull.* **2016**, *6*, 479–494. [CrossRef] [PubMed]
25. Izutsu, K.; Koida, T.; Takata, N.; Ikeda, Y.; Ono, M.; Inoue, M.; Fukami, T.; Yonemochi, E. Characterization and quality control of pharmaceutical cocrystals. *Chem. Pharm. Bull.* **2016**, *64*, 1421–1430. [CrossRef] [PubMed]
26. Kale, D.P.; Zode, S.S.; Bansal, A.K. Challenges in translational development of pharmaceutical cocrystals. *J. Pharm. Sci.* **2017**, *106*, 457–470. [CrossRef] [PubMed]
27. Lawson, J.D.; Sabat, M.; Scorah, N.; Smith, C.; Vu, P.H. Pyridinyl and fused pyridinyl triazolone derivatives. WO 2014/164558 A1, 9 October 2014.
28. Stella, J.S.; He, Q. Cyclodextrins. *Toxicol. Pathol.* **2008**, *36*, 30–42. [CrossRef]
29. Stahl, P.H.; Wermuth, C.G. Handbook of pharmaceutical salts properties, selection, and use. *Int. Union Pure Appl. Chem.* **2002**, *24*, 21.
30. Jantratid, E.; Janssen, N.; Reppas, C.; Dressman, J.B. Dissolution media simulating conditions in the proximal human gastrointestinal tract: An update. *Pharm. Res.* **2008**, *25*, 1663–1676. [CrossRef]
31. Tsutsumi, S.; Iida, M.; Tada, N.; Kojima, T.; Ikeda, Y.; Moriwaki, T.; Higashi, K.; Moribe, K.; Yamamoto, K. Characterization and evaluation of miconazole salts and cocrystals for improved physicochemical properties. *Int. J. Pharm.* **2011**, *421*, 230–236. [CrossRef]
32. Sheldrick, G. A short history of SHELXL. *Acta Crystallogr. Sect.* **2008**, *64*, 112–122. [CrossRef]
33. Kimoto, K.; Yamamoto, M.; Kitayama, M.; Sawai, Y.; Hohokabe, M.; Iwata, K. Cocrystal, Production Method Thereof, and Medicament Containing Cocrystal. WO 2017/111179 A1, 29 June 2017.
34. Alhalaweh, A.; Ali, R.H.H.; Velaga, S.P. Effects of polymer and surfactant on the dissolution and transformation profiles of cocrystals in aqueous media. *Cryst. Growth Des.* **2014**, *14*, 643–648. [CrossRef]
35. Saal, C.; Becker, A. Pharmaceutical salts: A summary on doses of salt formers from the Orange Book. *Eur. J. Pharm. Sci.* **2013**, *49*, 614–623. [CrossRef] [PubMed]
36. U.S. National Library of Medicine, U.S. Department of Health & Human Services. Available online: https://www.nlm.nih.gov/toxnet/index.html (accessed on 27 January 2020).
37. Paterson, J.R.; Blacklock, C.; Campbell, G.; Wiles, D.; Lawrence, J.R. The identification of salicylates as normal constituents of serum: A link between diet and health? *J. Clin. Pathol.* **1998**, *51*, 502–505. [CrossRef]
38. Boreham, D.R.; Martin, B.K. The kinetics of elimination of salicylic acid and the formation of gentisic acid. *Br. J. Pharmac.* **1969**, *37*, 294–300. [CrossRef]
39. Needs, C.J.; Brooks, P.M. Clinical pharmacokinetics of the salicylates. *Clin. Pharmacokinet.* **1985**, *10*, 164–177. [CrossRef] [PubMed]
40. Ashidate, K.; Kawamura, M.; Mimura, D.; Tohda, H.; Miyazaki, S.; Teramoto, T.; Yamamoto, Y.; Hirata, Y. Gentisic acid, an aspirin metabolite, inhibits oxidation of low-density lipoprotein and the formation of cholesterol ester hydroperoxides in human plasma. *Eur. J. Pharmacol.* **2005**, *513*, 173–179. [CrossRef] [PubMed]
41. Tehama, B.G.; Lloyd, E.J.; Wong, M.G.; Pitt, W.R.; Montana, J.G.; Manallack, S.T.; Gancia, E. Estimation of pKa using semi-empirical molecular orbital methods. part 1: Application to phenols and carboxylic acids. *Quant. Struct. Act. Relat.* **2002**, *21*, 457–472. [CrossRef]
42. Ando, S.; Kikuchi, J.; Fujimura, Y.; Ida, Y.; Higashi, K.; Moribe, K.; Yamamoto, K. Physicochemical characterization and structural evaluation of a specific 2:1 cocrystal of naproxen–nicotinamide. *J. Pharm. Sci.* **2012**, *101*, 3214–3221. [CrossRef]
43. Lorente, P.; Shenderovich, I.G.; Golubev, N.S.; Denisov, G.S.; Buntkowsky, G.; Limbach, H.H. $^{1}H/^{15}N$ NMR chemical shielding, dipolar 15N, 2Hcoupling and hydrogen bond geometry correlations in a novel series of hydrogen-bonded acid–base complexes of collidine with carboxylic acids. *Magn. Reson. Chem.* **2001**, *39*, S18–S29. [CrossRef]
44. Aakeröy, C.B.; Fasulo, M.E.; Desper, J. Cocrystal or salt: Does it really matter? *Mol. Pharm.* **2007**, *4*, 317–322. [CrossRef]
45. O'Driscoll, C.M. Lipid-based formulations for intestinal lymphatic delivery. *Eur. J. Pharm. Sci.* **2002**, *15*, 405–415.



© 2020 by the authors. Licensee MDPI, Basel, Switzerland. This article is an open access article distributed under the terms and conditions of the Creative Commons Attribution (CC BY) license (http://creativecommons.org/licenses/by/4.0/).